Micromagnetic modeling of critical current oscillations in magnetic Josephson junctions

I. A. Golovchanskiy,[1,2] V. V. Bol'ginov,[2,3] V. S. Stolyarov,[1,3,4,5] N. N. Abramov,[2] A. Ben Hamida,[2] O. V. Emelyanova,[6] B. S. Stolyarov,[5,7] M. Yu. Kupriyanov,[1,4,8] A. A. Golubov,[1,9] and V. V. Ryazanov[2,3,4,*]

[1]*Moscow Institute of Physics and Technology, State University, 9 Institutskiy per., Dolgoprudny, Moscow Region 141700, Russia*

[2]*National University of Science and Technology MISIS, 4 Leninsky prosp., Moscow 119049, Russia*

[3]*Institute of Solid State Physics (ISSP RAS), Chernogolovka, Moscow Region 142432, Russia*

[4]*Solid State Physics Department, Kazan Federal University, 420008 Kazan, Russia*

[5]*Faculty of Fundamental Physical and Chemical Engineering, M. V. Lomonosov Moscow State University, 1 Leninskie Gory, GSP-1, Moscow 119991, Russia*

[6]*National Research Nuclear University MEPhI, 31 Kashirskoye sh., Moscow 115409, Russia*

[7]*Scientific Production Enterprise Factor-TS, 11a 1st Magistralniy proezd, Moscow 123290, Russia*

[8]*M. V. Lomonosov Moscow State University, Skobeltsyn Institute of Nuclear Physics (SINP MSU), 1(2) Leninskie Gory, GSP-1, Moscow 119991, Russia*

[9]*Faculty of Science and Technology and MESA+ Institute for Nanotechnology, University of Twente, 7500 AE Enschede, The Netherlands*

(Received 28 September 2016; revised manuscript received 29 November 2016; published 21 December 2016)

In this work we propose and explore an effective numerical approach for investigation of critical current dependence on applied magnetic field for magnetic Josephson junctions with in-plane magnetization orientation. This approach is based on micromagnetic simulation of the magnetization reversal process in the ferromagnetic layer with introduced internal magnetic stiffness and subsequent reconstruction of the critical current value using total flux or reconstructed actual phase difference distribution. The approach is flexible and shows good agreement with experimental data obtained on Josephson junctions with ferromagnetic barriers. Based on this approach we have obtained a critical current dependence on applied magnetic field for rectangular magnetic Josephson junctions with high size aspect ratio. We have shown that the rectangular magnetic Josephson junctions can be considered for application as an effective Josephson magnetic memory element with the value of critical current defined by the orientation of magnetic moment at zero magnetic field. An impact of shape magnetic anisotropy on critical current is revealed and discussed. Finally, we have considered a curling magnetic state in the ferromagnetic layer and demonstrated its impact on critical current.

DOI: 10.1103/PhysRevB.94.214514

I. INTRODUCTION

Very recently, superconductor/ferromagnet hybrid structures based on weak ferromagnetic layers with low coercivity have regained strong practical interest due to their integration in various superconductor-ferromagnet-superconductor (SFS) Josephson spintronic elements [1–12] and superconducting ultrafast electronic devices [13,14].

Currently two major types of superconducting magnetic Josephson junctions (MJJs) are considered with out-of-plane or in-plane orientation of magnetization in the ferromagnetic (F) tunneling layer. Originally MJJs with out-of-plane magnetization based on the Nb-CuNi-Nb sandwich were the first used to observe supercurrent flow through the ferromagnetic Josephson barrier as well as for inversion of the Josephson current-phase relation (π state) [9,15–17]. However, due to stable magnetic domain structure (relatively high coercive field) and out-of-plane magnetic anisotropy, the Cu-Ni-based MJJs are useful only for fabrication of the superconducting phase inverters with constant phase shifts employed in digital [15,16] and quantum [16,18] logic.

In contrast, Pd-Fe alloy thin films with small Fe content exhibit in-plane magnetization and small coercive field making them perfect candidates for application in novel ultrafast Josephson cryogenic magnetic memory [4–7]. The value of the critical current of the MJJ memory element is defined by in-plane magnetic flux including magnetization of the F layer and, therefore, is governed by magnetic history of the ferromagnetic layer.

In this work we propose and explore an effective numerical approach for investigation of critical current dependence on applied magnetic field for Josephson junctions with a ferromagnetic barrier possessing in-plane magnetization orientation. The method is based on micromagnetic simulation of the magnetization reversal process in the ferromagnetic barrier and subsequent derivation of the critical current employing magnetic flux or numerically reconstructed distribution of the Josephson phase difference. We focus on $Pd_{0.99}Fe_{0.01}$-based MJJs. Yet, the method can be applied to any MJJ with in-plane magnetization in a ferromagnetic tunnel barrier.

This paper is organized as follows. In Sec. II we provide details for a reconstruction procedure of the Fraunhofer-like critical current dependence on applied magnetic field based on micromagnetic simulation. Micromagnetic simulation justifies a finite hysteresis loop by nonalignment of orientations of local magnetic moments with applied magnetic field. To our best knowledge, the only attempt to discuss the finite hysteresis loop of the $Pd_{0.99}Fe_{0.01}$ tunnel barrier considering realignment of local magnetic moments was done in Ref. [7], but for a simplified 1D case and employing a Gaussian probability density for a flip of the local moment in applied magnetic field. In Sec. III we derive the Fraunhofer-like critical current curves for rectangular MJJs and discuss their applicability as a Josephson memory element. Digital states of a rectangular

*Corresponding author: ryazanov@issp.ac.ru

memory element are associated with orientation of a saturated magnetic moment along or across the long side of MJJs. Originally, determination of the logical state of the MJJ memory element via orientation of magnetic moment was proposed theoretically in Refs. [19,20] but for a complex mixed 0-π MJJ. In Sec. IV we enforce a curling distribution of local magnetic moments in the F barrier and discuss its effect on critical current highlighting the difference between approaches of critical current derivation. In Sec. V we provide a summary and give several concluding remarks on further development of magnetization reversal simulation and magnetic memory based on magnetic Josephson junctions.

II. RECONSTRUCTION OF CRITICAL CURRENT OF MJJ (VERIFICATION OF THE MODEL)

A. Critical current dependence on applied magnetic field of MJJ

Experimental critical current dependencies on applied magnetic field $[I_c(H)]$ are shown in Fig. 1(a) for a 10×10 μm^2 superconductor-ferromagnet-superconductor (SFS) magnetic Josephson junction (MJJ) and in Fig. 1(b) for a 10×10 μm^2 superconductor-insulator-superconductor-ferromagnet-superconductor (SIsFS) MJJ. These MJJs are of a lumped type implying an $l \ll \lambda_J$ limit, where l is an in-plane size of a junction and λ_J is a Josephson penetration depth of the MJJ. The experimental data in Figs. 1(a) and 1(b) were reported previously in Refs. [4] and [6], respectively, and are normalized with respect to the maximum I_c. For convenience, we refer further to the experimental result shown in Fig. 1(a) as MJJ_1 and to the one shown in Fig. 1(b) as MJJ_2. Fabrication and measurement details for these MJJs can be found elsewhere [4,6,21]. A comprehensive theory of operation principles of SIsFS spintronic devices can be found in Refs. [7,22] and references therein. Only the $I_c(H)$ curves at positively swept magnetic field are shown, since the $I_c(H)$ at negatively swept field are its mirror reflections with respect to the $H = 0$ axis. As discussed in Refs. [4,6,7,21], the $I_c(H)$ dependence of MJJs with in-plane orientation of magnetic moment in the F layer is represented by a Fraunhofer-like pattern shifted from zero field in accordance with the hysteresis dependence of magnetization of the F layer on magnetic field $[M(H)]$. In particular, the maximum of $I_c(H)$ corresponds to a zero total magnetic flux across the MJJ and is located at the magnetic field value of the same sign as the sweep of the magnetic field [i.e., the maximum of $I_c(H)$ is observed at positive H for positive magnetic field sweep and vice versa] since the magnetization of the F layer contributes to magnetic flux. This magnetic memory effect is a key feature of MJJs with in-plane orientation of magnetic moment making such MJJs applicable as a Josephson magnetic memory element.

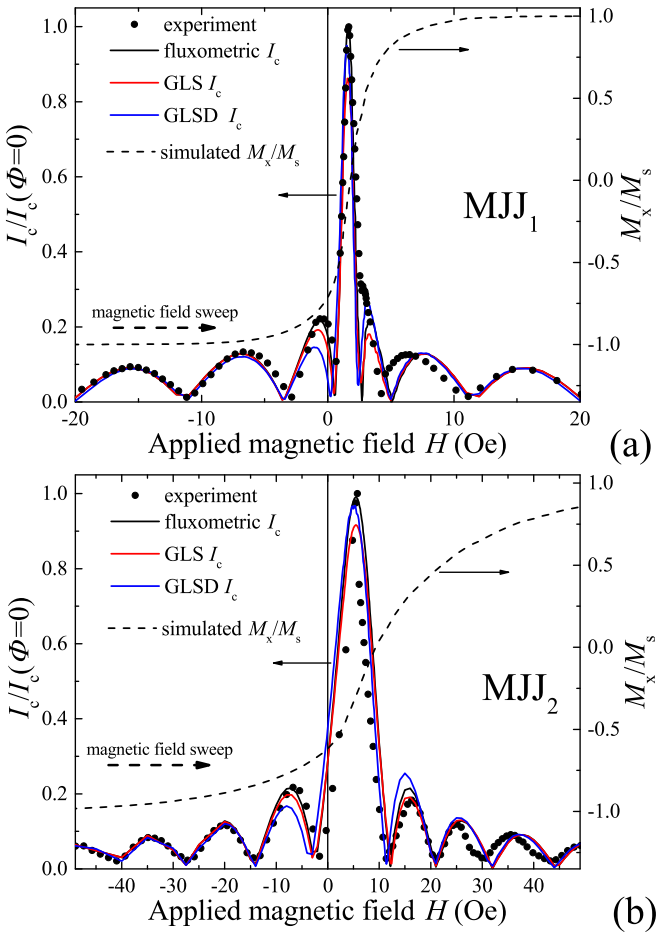

FIG. 1. Experimental and reconstructed dependencies of the critical current on applied magnetic field for 10×10 μm^2 size MJJ_1 SFS (a) and MJJ_2 SIsFS (b). The I_c is normalized by the maximum critical current $I_c(\Phi = 0)$ (i.e., by I_c at zero total magnetic flux). Dashed lines show corresponding dependencies of the mean magnetization of the F layer on applied magnetic field. The mean magnetization is normalized by the saturation magnetization M_s.

At magnetic field well above the saturation field of the F layer, the $I_c(H)$ dependence can be easily fitted [4,6] with the classical Fraunhofer dependence valid for rectangular-shaped lumped junctions:

$$I_c = \left|\frac{\sin(\pi\Phi_x/\Phi_0)}{\pi\Phi_x/\Phi_0}\right|\left|\frac{\sin(\pi\Phi_y/\Phi_0)}{\pi\Phi_y/\Phi_0}\right|. \quad (1)$$

In Eq. (1), Φ_0 is the magnetic flux quantum, Φ_x is the total magnetic flux in the x direction across the junction of width a, and Φ_y is the total magnetic flux in the y direction across the junction of length b:

$$\Phi_x(\vec{H}) = H_x a d_m + M_x(\vec{H}) a d_f,$$
$$\Phi_y(\vec{H}) = H_y b d_m + M_y(\vec{H}) b d_f. \quad (2)$$

In Eq. (2), d_m is the magnetic thickness [4,6,7], d_f is a fabrication-defined thickness of the magnetic layer, $H_{x,y}$ are the components of the applied magnetic field, and $M_{x,y}$ are the components of magnetization of the F barrier. The thicknesses of magnetic layers are $d_f = 30$ nm for MJJ_1 and $d_f = 15$ nm for MJJ_2. Commonly, magnetic field is applied along a principal axis (i.e., $H_x = H$ and $H_y = 0$) and at magnetic field well above the saturation field $M_x(H) = M_s = \text{constant}$, $M_y(H) = 0$, implying $\Phi_y = 0$. The fitting procedure performed in Refs. [4,6] yields $M_s = 9.5\times10^4$ A/m, $d_m = 230$ nm for MJJ_1 and $M_s = 13.5\times10^4$ A/m, $d_m = 139$ nm for MJJ_2. In order to fit the $I_c(H)$ at magnetic field below the saturation field where the magnetization reversal of the F layer takes place the

$M_x(H)$ dependence can be interpolated by arctangent [4,6] or any other suitable analytical sigmoid-like function [7].

B. Micromagnetic model of $Pd_{0.99}Fe_{0.01}$ F layer

A true $\vec{M}(\vec{H})$ dependence for the F layer at $|\vec{H}|$ below the saturation field can be obtained performing a micromagnetic simulation of the magnetization reversal process in the $Pd_{0.99}Fe_{0.01}$ tunneling layer. Micromagnetic simulation [23] is based on numerical simulation of the Landau-Lifshitz-Gilbert equation for local unit macrospin vectors $\vec{m} = \vec{m}(x,y)$ placed in local reduced effective magnetic fields $\vec{h}_{\rm eff} = \vec{h}_{\rm eff}(x,y)$:

$$\frac{d\vec{m}}{d\tilde{t}} = \vec{m} \times \vec{h}_{\rm eff} + \alpha \vec{m} \times \vec{m} \times \vec{h}_{\rm eff}, \tag{3}$$

where time scale $\tilde{t}$ is unitless and is reduced as $\tilde{t} = t\gamma_0 M_s/(1+\alpha^2)$, γ_0 is the gyromagnetic ratio, M_s is the saturation magnetization of a simulated ferromagnet, and α is the Gilbert damping constant [24]. In Eq. (3), both $\vec{m}$ and $\vec{h}_{\rm eff}$ are reduced with M_s. Field $\vec{h}_{\rm eff}$ typically includes reduced applied magnetic field $\vec{h}$, reduced field of local macrospin interaction $\vec{h}_{\rm loc}$, reduced field of magnetostatic interaction $\vec{h}_d$, and reduced anisotropy field $\vec{h}_a$:

$$\vec{h}_{\rm eff} = \vec{h} + \vec{h}_{\rm loc} + \vec{h}_a + \vec{h}_d. \tag{4}$$

Yet, accurate micromagnetic simulation of magnetization reversal in the $Pd_{0.99}Fe_{0.01}$ F layer can hardly be performed in the conventional manner due to the complex cluster nature of magnetism in $Pd_{0.99}Fe_{0.01}$ [25]. The magnetic moment of the $Pd_{0.99}Fe_{0.01}$ thin film is distributed mostly within the relatively large Fe-rich Pd_3Fe nanoclusters of $\sim$10 nm size and $\sim$100 nm spacing in between. The clusters are embedded in a paramagnetic host layer. A finite hysteresis loop derived in Refs. [4,6,25] is justified by reorientation of the magnetic moment of these clusters. The paramagnetic host can be saturated only at high magnetic field $H > 1$–2 kOe [25] and, therefore, does not contribute to the $M(H)$ hysteresis dependence in our field of interest. In particular, typical hysteresis loops derived from experiments with $Pd_{0.99}Fe_{0.01}$-based MJJs do not demonstrate the paramagnetic component. Also, it is practically impossible for micromagnetic simulation to account for (i) the essentially granular structure of $Pd_{0.99}Fe_{0.01}$ films integrated in the considered MJJs [24] and (ii) the large typical in-plane size of the F layer of $\sim$10 μm, which is particularly large for meshing it with appropriate cell size and number of cells.

Considering the physical picture of magnetization in the $Pd_{0.99}Fe_{0.01}$ F barrier, we propose the following modification for the standard micromagnetic approach. We divide the $10\times10\times d_f$ μm^3 F layer into a 2D mesh of $\Delta x \times \Delta y \times \Delta z = 100\times100\times d_f$ nm^3 cells ($100\times100\times1$ mesh). Each cell contains at least one Fe-rich cluster of saturation magnetization $M_{\rm Pd_3Fe} \simeq 5\times10^5$ A/m. The orientation of the micromagnetic macrospin in each cell $\vec{m}(x,y)$ in Eq. (3) corresponds to the orientation of the magnetic moment in the Fe-rich cluster. Thus, values of local magnetization in Eq. (3) and effective field components in Eq. (4) are reduced with $M_{\rm Pd_3Fe}$. On the other hand, the magnetic moment of the entire cell corresponds to the mean magnetic moment M_s extracted from the fitting procedure of the experimental Fraunhofer pattern. This magnetic moment contributes to measured magnetization and, therefore, to magnetic flux across MJJs.

Within the proposed model the terms of effective field in Eq. (4) are modified as follows. The macrospin orientation of each cell $\vec{m}(x,y)$ is engaged with surrounding cells of magnetic moment M_s via standard magnetostatic interaction with magnetostatic field $\vec{h}_d$ and local interaction with effective field $\vec{h}_{\rm loc}$. The reduced magnetostatic field $\vec{h}_d(x,y) = \vec{H}_d(x,y)/M_{\rm Pd_3Fe} = -\sum \mathbf{N}(x-x_1, y-y_1)\vec{m}(x_1,y_1) \times M_s/M_{\rm Pd_3Fe}$, where $\mathbf{N}$ is the demagnetizing tensor [26] and the summation is performed over the entire F barrier. The normalized local field $\vec{h}_{\rm loc}(x,y) = \vec{H}_{\rm loc}(x,y)/M_{\rm Pd_3Fe} = 2A/(\mu_0 M^2_{\rm Pd_3Fe})\nabla^2\vec{m}(x,y) \times M_s/M_{\rm Pd_3Fe}$, where ∇^2 is the Laplace operator and the exchange stiffness constant $A = 1\times10^{-11}$ J/m is of a typical order for Fe-based alloys including Pd_3Fe. We employ standard Newman boundary conditions for $\vec{h}_{\rm loc}(x,y)$ calculation. In simple terms, both standard reduced fields $\vec{h}_d$ and $\vec{h}_{\rm loc}$, which act on macrospin of orientation $\vec{m}(x,y)$ and of magnetization $M_{\rm Pd_3Fe}$, are scaled by the ratio $M_s/M_{\rm Pd_3Fe}$. The external field in each cell is also reduced with $M_{\rm Pd_3Fe}$: $\vec{h}(x,y) = \vec{H}/M_{\rm Pd_3Fe}$.

Finally we introduce an internal magnetic stiffness (IMS). The IMS is a static property which justifies phenomenologically the resilience of the entire F layer to the remagnetization. Incorporation of the IMS into the micromagnetic model is required for quantitative justification of the experimentally observed finite hysteresis loop width of the $Pd_{0.99}Fe_{0.01}$ F barrier. The IMS may result from variation of size and/or shape of Fe-rich clusters, their noncentral location within the individual cell, certain easy magnetization axes arbitrarily oriented for each cluster, or pinning of macrospin orientation in granular medium. We represent the IMS by random anisotropy vectors in each cell $H_s\vec{R}(x,y)$, where $\vec{R}(x,y)$ are random vectors of normally distributed length and uniformly distributed orientation, and H_s is the magnetic stiffness constant. Thus, the IMS acts in our model as a randomly distributed anisotropy field $\vec{h}_a(x,y) = \vec{H}_a(x,y)/M_{\rm Pd_3Fe} = \vec{R}(x,y)\vec{m}(x,y) \times H_s/M_{\rm Pd_3Fe}$. Such approach is referred to commonly as the random anisotropy model [27–29], developed originally for amorphous and nanostructured ferromagnets.

Introduction of the IMS and employment of large cell size make our micromagnetic simulation unable to obtain fine magnetic structure of the F layer. Yet, they allow us to reveal a macroscopic curling distribution of magnetization, such as flower, vortex, or S states, if any appears. Also, the model enables magnetization reversal at experimentally defined coercive field. The value of magnetic stiffness constant H_s is an extra free-fitting parameter in our micromagnetic approach defined experimentally.

Derivation of a hysteresis loop is performed as follows. At each magnetic field step H, Eq. (3) is relaxed using a second-order Runge-Kutta numerical scheme until the convergence is reached. A unitless convergence criterion is set as $d\vec{m}/d\tilde{t} < 10^{-7}$. We set $\alpha = 0.5$ for faster convergence. At each magnetic field step, the final averaged orientation of magnetic moments defines the corresponding magnetization of the F barrier at magnetic field H: $M_{x,y}(H) = \langle m_{x,y}(x,y,H)\rangle M_s$. Magnetic field was swept from -50 Oe to 50 Oe with a progressive field step. A leap-frog scheme is employed where the resulting

$\vec{m}(x,y)$ distribution at the previous field step is used as the initial one at the next field step.

C. Reconstruction methods

In order to obtain H_s for F layers of MJJ_1 and MJJ_2, we run a series of hysteresis loop simulations for corresponding F-layer geometries and magnetic parameters varying the H_s. We found that coercive force is in approximately linear dependence with H_s. At $H_s/M_{Pd_3Fe} = 11.5\times10^{-4}$ and $H_s/M_{Pd_3Fe} = 5\times10^{-3}$ zero total magnetic flux is obtained at $H = 1.65$ Oe and $H = 5.76$ Oe for MJJ_1 and MJJ_2, respectively, corresponding to a maximum of $I_c(H)$ observed in experiment (Fig. 1). The dashed lines in Fig. 1 show the branches of hysteresis $M_x(H)$ dependencies in positively swept magnetic field. The factor of 4 difference in H_s parameters for MJJ_1 and MJJ_2 is attributed to the same difference factor in coercive field.

Once the exact $\vec{M}(\vec{H})$ is calculated for F layers the corresponding $I_c(\vec{H})$ can be restored directly using Eqs. (1) and (2). Since this reconstruction of critical current implies calculation of the total magnetic flux along and across the applied magnetic field we refer to this approach as fluxometric reconstruction of $I_c(\vec{H})$ dependence. The fluxometric reconstructed $I_c(H)$ for MJJ_1 and MJJ_2 are shown with black lines in Figs. 1(a) and 1(b), respectively, demonstrating a good match with the experimental data.

An exact $I_c(\vec{H})$ dependence for a lumped MJJ can be obtained using a distribution of a phase difference $\varphi(x,y,\vec{H})$ as follows:

$$I_c(\vec{H}) = \max\left[\int_{b/2}^{-b/2}\int_{a/2}^{-a/2}\sin\varphi(x,y,\vec{H})dxdy\right], \qquad (5)$$

where the phase difference is determined by the following gradient distribution:

$$\frac{d\varphi(x,y,\vec{H})}{dx} = H_y d_m + \left[m_y(x,y,\vec{H}) + h_d^y(x,y,\vec{H})\right]M_s d_f,$$
$$\frac{d\varphi(x,y,\vec{H})}{dy} = H_x d_m + \left[m_x(x,y,\vec{H}) + h_d^x(x,y,\vec{H})\right]M_s d_f, \qquad (6)$$

where $H_{x,y}$ are the components of applied magnetic field, and $h_d^{x,y}(x,y,\vec{H})$ are the local demagnetizing field components.

The fluxometric reconstruction [Eqs. (1), (2)] is only a limiting case for exact $I_c(\vec{H})$ dependence [Eqs. (5), (6)] of rectangular MJJ in approximation of uniform field and $\vec{m}(x,y,\vec{H})$ distribution. The major significance of micromagnetic simulated magnetization reversal in the F layer is the derivation of local magnetic moments at each field step $\vec{m}(x,y,\vec{H})$. These moments can be employed for determination of the phase difference distribution using Eq. (6) if a limiting condition for a micromagnetic cell size $\xi < \Delta x \ll \lambda_J$ is fulfilled, where ξ is the superconducting coherence length. Derivation of a scalar field $\varphi(x,y,\vec{H})$ from a known distribution of its gradient is a well-known Poisson problem. In applied mathematics, reconstruction of a scalar field from its gradient is widely used in photometric stereo or shape from shading analysis [30,31]. Importantly, current numerical approaches allow us to reconstruct a scalar field from a nonintegrable gradient which contains noise, nonzero curl, and in absence of boundary conditions. Red lines in Figs. 1(a) and 1(b) show the $I_c(H)$ for MJJ_1 and MJJ_2, respectively, derived from Eq. (5) using a global least-squares (GLS) reconstruction algorithm for phase difference distribution $\varphi(x,y,H)$ [Eq. (6)]. The GLS-reconstructed $I_c(H)$ shows a good fit with experimental data and fluxometric reconstruction. Yet, the maximum of $I_c(H)$ is reduced to 0.86 for MJJ_1 and 0.92 for MJJ_2. The reduction is related to partial relaxation of local macrospins along $\vec{H}_a(x,y)$ at $\vec{\Phi} = 0$. If the boundary conditions for the Poisson problem are known, the phase difference reconstruction can be performed using a GLS reconstruction algorithm with Dirichlet boundary conditions (GLSD). We consider linearized boundary conditions which set a total tilt of a phase difference surface according to $\Phi_x(H)$ and $\Phi_y(H)$ [see Eq. (2)]. The GLSD-reconstructed $I_c(H)$ are also shown in Figs. 1(a) and 1(b) for MJJ_1 and MJJ_2, respectively, with blue lines, demonstrating a good match with the experiment and both fluxometric and GLS-reconstructed $I_c(H)$ dependencies. Successful GLSD reconstruction of critical current indicates applicability of linearized boundary conditions for the Poisson problem.

III. RECTANGULAR MJJ MEMORY ELEMENT

The main purpose of this work is the development of the approach for numerical analysis of critical current dependence on applied magnetic field for MJJs with in-plane magnetization orientation. Once a single successful measurement of Fraunhofer $I_c(H)$ dependence on MJJ is carried out, the micromagnetic parameters can be derived using the procedure discussed in Sec. II. If the fabrication process and measurement temperature are reproducible, these parameters will remain for all geometries of MJJ, validating the reconstructed $I_c(H)$ for a proposed geometry. This gives an opportunity to design the MJJ memory element with a desired response numerically instead of performing multiple labor-intensive experiments.

As a demonstration, we consider two MJJs with magnetic parameters corresponding to MJJ_1 and MJJ_2 but of size $12\times4\ \mu m^2$. The smallest size of 4 μm is chosen as the smallest comfortable size for a conventional optical lithography, while the largest size 12 μm is chosen to provide a sufficient aspect ratio of a factor of 3. Figures 2(a) and 2(b) show $I_c(H)$ dependencies and corresponding $M_{x,y}(H)$ curves for MJJ_1 and MJJ_2 of $12\times4\ \mu m^2$ size, respectively, obtained by applying magnetic field in the x direction along the long side ($\alpha = 0^\circ$) and in the y direction across the long side ($\alpha = 90^\circ$).

The rectangular shape of MJJs enables us to use the dependence of oscillation period of Fraunhofer critical current pattern $I_c(H)$ on orientation of applied magnetic field. Indeed, the oscillation period of $I_c(H)$ is defined by the magnetic surface ad_m and ad_f [see Eq. (2)]. When the magnetic field is applied across the short side ($\alpha = 0^\circ$ in Fig. 2), the $I_c(H)$ varies slowly with H and at $H = 0$ critical current remains high. In particular, $I_c(H = 0) \simeq 0.6$ for MJJ_1 and $I_c(H = 0) \simeq 0.8$ for MJJ_2. When the magnetic field is applied across the long side ($\alpha = 90^\circ$ in Fig. 2), the $I_c(H)$ varies rapidly with H since the magnetic surface is increased by a factor of 3. For MJJ_1 at $H = 0$ fluxometric and GLS-reconstructed $I_c(H = 0) \simeq 0.2$ and GLSD-reconstructed $I_c(H = 0) \simeq 0.05$. For MJJ_2 at $H = 0$ fluxometric, GLS-, and GLSD-reconstructed $I_c(H = 0) \simeq 0.2$. We argue that the size of rectangular MJJ can always be

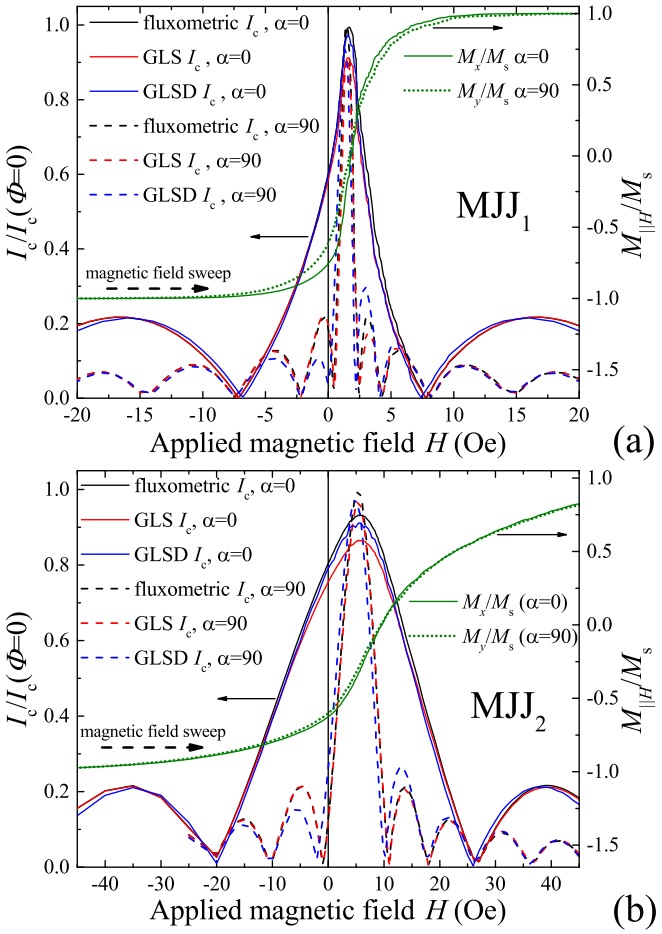

FIG. 2. Micromagnetic reconstructed dependencies of critical current on applied magnetic field for 12×4 μm^2 size MJJ$_1$ SFS (a) and MJJ$_2$ SIsFS (b) and magnetic field orientation along the long size ($\alpha = 0^\circ$) and across the long size ($\alpha = 90^\circ$). Green lines show corresponding field dependencies of mean magnetization aligned with the applied magnetic field ($M_{||H}$).

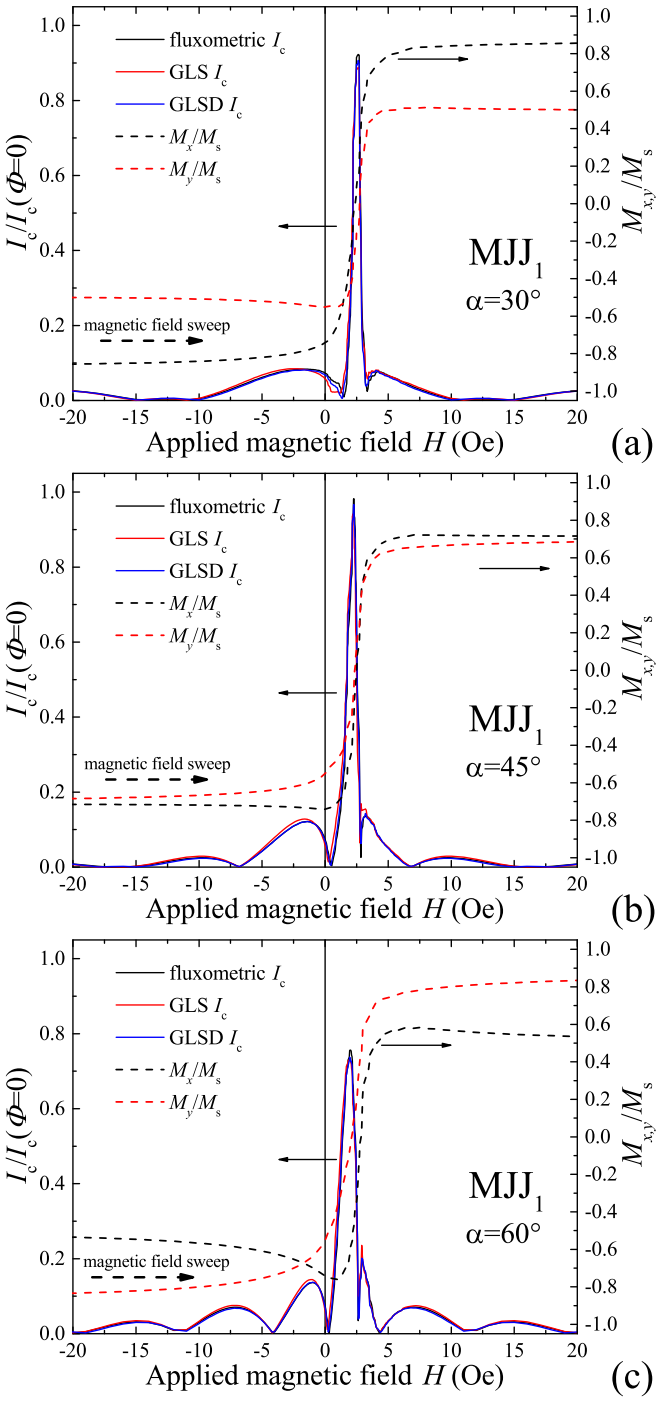

FIG. 3. Micromagnetic reconstructed dependencies of critical current on applied magnetic field for 12×4 μm^2 size MJJ$_1$ SFS and magnetic field applied at $\alpha = 30^\circ$ (a), $\alpha = 45^\circ$ (b), and $\alpha = 60^\circ$ (c). Dashed lines show field dependencies of corresponding projections of magnetization on principal axes.

chosen in such a way that at $\alpha = 90^\circ$ the $I_c(H = 0) \simeq 0.0$ corresponding to $\vec{\Phi}(H) = \Phi_0$ condition for the first minimum of the Fraunhofer pattern.

It appears that the rectangular MJJs can be convenient for application as a memory element for Josephson magnetic memory where the logical state is defined by the orientation of saturated magnetization in the absence of applied magnetic field. A write operation for the rectangular memory element is realized by applying a magnetic field pulse of a constant amplitude, but selective (x or y) orientation. The amplitude of the write pulse should be sufficient to saturate the magnetic moment of the F layer in any x ($\alpha = 0^\circ$) or y direction ($\alpha = 90^\circ$). The pulse aligned with the x direction records logical 0, while one aligned with the y direction records logical 1. As an example, the amplitude of the pulse of $H > 15$ Oe is sufficient to perform the write operation for MJJ$_1$ of 12×4 μm^2 size [Fig. 2(a)]. A readout operation is performed by applying a readout current (I_r). The value of I_r for the rectangular memory element is defined in between $I_c(H = 0, \alpha = 0^\circ)$ and $I_c(H = 0, \alpha = 90^\circ)$. A value $I_r = 0.4 I_c(\Phi = 0)$ can be used for the MJJ$_1$ memory element [Fig. 2(a)]. If the logical 1 is recorded, the readout current exceeds the critical current [$I_r > I_c(H = 0)$] and a voltage signal appears. If the logical 0 is recorded, $I_r < I_c(H = 0)$ and the memory element remains in the superconducting state. Importantly, Fig. 2 shows that the difference in critical currents for $\alpha = 0^\circ$ and $\alpha = 90^\circ$ orientations at $H = 0$ reaches a factor of 3–4, which provides a clear difference between the two logical states.

The realization of logical states via orientation of saturated magnetization in rectangular MJJ at $H = 0$ might be more practical than square MJJs. The Fraunhofer patterns of square MJJs are absolutely identical with respect to the orientation of magnetic field along principal axes. Hence, in order to realize the distinct logical states in the square MJJ, some additional means are required: the square MJJ should operate under external or self-field magnetic bias [21]. Besides, partial hysteresis loops can be used for square memory elements [4,5], but this requires magnetic field pulses of different amplitudes for the write operation in the square element, which complicates the magnetic recording protocol. A rectangular MJJ memory element with the magnetization-orientation-defined logical states does not possess these disadvantages.

Also, the role of magnetic shape anisotropy in magnetization reversal of the F layer is well pronounced for MJJ_1 in Fig. 2(a): the remanent magnetization $M(H = 0) \simeq 0.76$ at $\alpha = 0^\circ$ and $M(H = 0) \simeq 0.6$ at $\alpha = 90^\circ$. In particular, sharp reversal of magnetization at $\alpha = 0^\circ$, caused by the shape anisotropy, is partially responsible for concavity of central Fraunhofer maximum. In contrast, magnetic shape anisotropy of MJJ_2 does not play any role, since both $M_x(H)$ and $M_y(H)$ curves in Fig. 2(b) coincide.

The micromagnetic model allows us to derive $\vec{M}(\vec{H})$ curves and corresponding $I_c(\vec{H})$ for MJJs at arbitrary angles of applied magnetic field. Figure 3 shows $I_c(H)$ dependencies and corresponding $M_{x,y}(H)$ curves for MJJ_1 of 12×4 μm^2 size obtained by applying magnetic field at $\alpha = 30^\circ$, $\alpha = 45^\circ$, and $\alpha = 60^\circ$. An exact match for all three reconstruction methods is demonstrated. Interestingly, the state $\Phi = 0$ with $I_c = 1$ is reached at $\alpha = 45^\circ$ only where simultaneously $\Phi_x = 0$ and $\Phi_y = 0$, while at $\alpha = 30^\circ$ $\max(I_c) \simeq 0.9$ and at $\alpha = 60^\circ$ $\max(I_c) \simeq 0.74$. For all three angles of the applied magnetic field $I_c(H = 0) < 0.1$. Also, a narrow first minimum of sub-Oe width is noticeable at $H \simeq 2.5$ Oe for $\alpha = 45^\circ$ and $\alpha = 60^\circ$ which will be complicated to resolve experimentally. Importantly, the progress of $M_x(H)$ and $M_y(H)$ curves, i.e., a minor drop of $M_y(H)$ at $H \simeq 0$ in Fig. 3(a) and of $M_x(H)$ at $H \simeq 0$ best seen in Fig. 3(c), demonstrates an attempt of alignment of local macrospins along principal axes of the F layer and indicates magnetization reversal through a so-called S state. Such behavior of $M_{x,y}(H)$ curves as well as the mismatch of coercive field for M_x and M_y [best seen in Fig. 3(c)] imply a contribution of the shape anisotropy to magnetization reversal process. The impact of the shape anisotropy makes micromagnetic simulation irreplaceable for accurate $I_c(H)$ determination.

Figure 4 shows $I_c(H)$ dependencies and corresponding $M_{x,y}(H)$ curves for MJJ_2 of 12×4 μm^2 size obtained by applying magnetic field at $\alpha = 45^\circ$. The state with $\Phi = 0$ is also reached at $H \simeq 8$ Oe. In contrast to MJJ_1 (Fig. 3), both $M_x(H)$ and $M_y(H)$ curves coincide indicating a complete dominance of the IMS in magnetization reversal with no impact of the shape anisotropy. This result implies that, technically, no micromagnetic reconstruction is required for MJJ_2 junction: the $I_c(H)$ can always be obtained using fluxometric reconstruction with interpolated analytically $M_{x,y}(H)$ curves. The interpolated $M_{x,y}(H)$ curves will maintain for all in-plane orientations of magnetic field and reasonable variation of in-plane sizes.

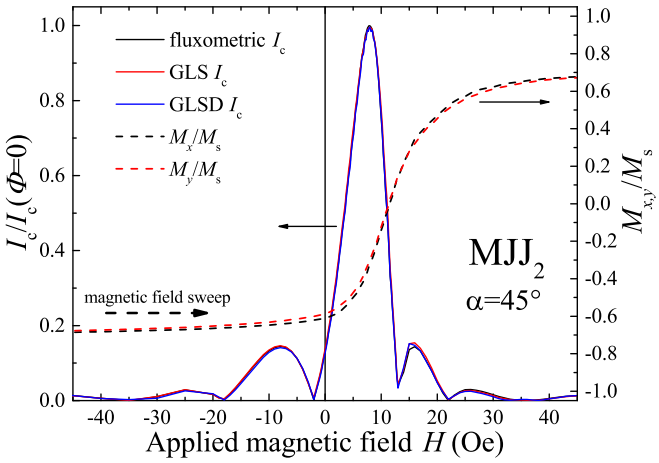

FIG. 4. Micromagnetic reconstructed dependencies of critical current on applied magnetic field for 12×4 μm^2 size MJJ_2 SIsFS and magnetic field orientation $\alpha = 45^\circ$. Dashed lines show field dependencies of corresponding projections of magnetization on principal axes.

Thus, two limits for 12×4 μm^2 rectangular MJJs are presented. In the first limit [MJJ_1; Figs. 2(a) and 3], the shape anisotropy of the F layer does play a significant role in magnetization reversal and in accurate determination of $I_c(\vec{H})$. In the second limit [MJJ_2; Figs. 2(b) and 4], the impact of the shape anisotropy is suppressed by the IMS. One can derive the criteria of necessity for micromagnetic simulation of magnetization reversal as follows. A simple estimation of the shape anisotropy field H_{SA} for a rectangular thin-film element [32–35] of a length a along the applied magnetic field, width b, and thickness c, $H_{SA}/M_{Pd_3Fe} \sim c(\sqrt{4a^2+b^2} - b)/(\pi ab) \times M_s/M_{Pd_3Fe}$, yields $H_{SA}/M_{Pd_3Fe} \sim 8\times10^{-4}$ for $12\times4\times0.03$ μm^3 MJJ_1 and $H_{SA}/M_{Pd_3Fe} \sim 5\times10^{-4}$ for $12\times4\times0.015$ μm^3 MJJ_2. These values can be compared with corresponding magnetic stiffness parameters (11.5×10^{-4} for MJJ_1 and 5×10^{-3} for MJJ_2). The magnetic stiffness dominates the magnetization reversal process for MJJ_2 where $H_{SA}/M_{Pd_3Fe} \ll H_s/M_{Pd_3Fe}$. In this case the fluxometric reconstruction with the interpolated $M_{x,y}(\vec{H})$ will provide a correct $I_c(\vec{H})$ dependence for all in-plane orientations of magnetic field and reasonable variation of in-plane sizes, since the interpolated $M_{x,y}(\vec{H})$ will hold.

In contrast, the shape anisotropy plays a significant role for MJJ_1 where $H_{SA}/M_{Pd_3Fe} \gtrsim H_s/M_{Pd_3Fe}$ and micromagnetic simulation is required for $I_c(\vec{H})$ determination.

IV. CRITICAL CURRENT OF MJJ WITH F LAYER AT CURLING STATE

We should note that since the fluxometric reconstruction [Eqs. (1), (2)] is a limiting case for exact $I_c(H)$ dependence [Eqs. (5), (6)] of rectangular MJJs, it might not be able to show an adequate $I_c(H)$ dependence in special cases even for rectangular shape. In particular, the fluxometric reconstruction considers that the distribution $\varphi(x, y, H) = \text{constant} = 0$ at $\vec{\Phi} = 0$. Yet, if deposition of the F layer is performed at high enough temperature or the MJJ is annealed at a certain

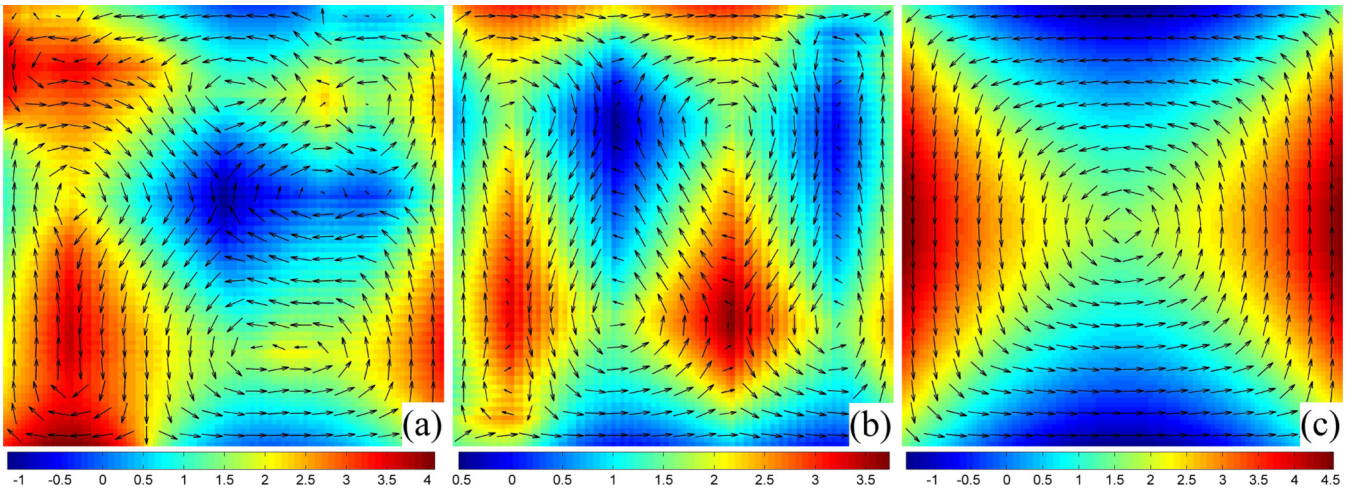

FIG. 5. Distributions of magnetic moment (arrows) and phase difference (color map) in the F layer corresponding to MJJ_1 SFS but in absence of the internal magnetic stiffness (i.e., $H_s = 0$) at $H = 0$. (a) The state is obtained from initially random distribution of magnetic moment. (b) The state is obtained from initial distribution of magnetic moment saturated away from the principal axes. (c) The state is obtained from initially curled distribution. Phase difference color scales are shown at the bottom.

fabrication stage the internal magnetic stiffness induced by the magnetic structure of the F layer may vanish. In this case the magnetization reversal process of an F layer of such size will occur through a curling kind of state such as the well-known S, C, or vortex magnetic states. The curling state can be characterized by a well-defined macroscopic distribution of magnetization orientation which in general violates the $\varphi(x,y,H) = 0$ condition at $\vec{\Phi} = 0$.

In order to highlight the difference between fluxometric and GLS reconstruction methods, we consider the original MJJ_1 junction of 10×10 μm^2 size with corresponding magnetic properties of a 30 nm F layer but in the absence of the IMS. Since the internal magnetic stiffness is absent, magnetization of the F layer might relax completely ($\vec{M} = 0$) at $H = 0$ providing fluxometric $\vec{\Phi} = 0$ and $I_c = 1$ according to Eqs. (1) and (2). On the other hand, a certain distribution of local moments $\vec{m}(x,y)$ in the F layer might reduce the I_c according to Eqs. (5) and (6).

The relaxed distribution of magnetization at $H = 0$ is initial-condition sensitive. Therefore, we consider three typical cases of initial $\vec{m}(x,y)$ distribution which can be obtained experimentally. Figure 5(a) shows a distribution of local magnetic moments and corresponding phase difference in a tunneling F layer relaxed from initially random orientations of macrospin unit vectors. This complex state can be obtained by zero-field-cooling the MJJ through the Curie temperature of the F layer and is characterized by several vortex-like and domain-wall-like eddies. Typically, the magnetic moment of the F layer relaxed from random initial conditions is $|\vec{M}|/M_s < 10^{-1}$. In a particular case, shown in Fig. 5(a), $|\vec{M}|/M_s \sim 10^{-2}$ yields fluxometric $I_c \simeq 0.98$. At the same time, the curling distribution of magnetization yields GLS $I_c \simeq 0.58$, i.e., by the factor of almost 2 smaller.

Figure 5(b) shows a distribution of local magnetic moments and corresponding phase difference in the tunneling F layer relaxed from the saturated state aligned at a small angle of 1° relative to the x axis. This state can be obtained by applying large magnetic field at the corresponding angle and reducing it to zero. Typically, any state we have obtained from the initially saturated one at any angle away from the principal axes can be characterized by an even number of vortex-like and domain-wall-like eddies and remanent magnetization $|\vec{M}|/M_s > 10^{-1}$. In a particular case, shown in Fig. 5(b), $|\vec{M}|/M_s \sim 10^{-1}$ yields fluxometric $I_c \simeq 0.85$. The fluxometric I_c is reduced due to the presence of substantial $M_{x,y}$ components. At the same time, the curling distribution of magnetic moment orientations yields GLS $I_c \simeq 0.76$. A smaller difference between fluxometric and GLS-reconstructed I_c is justified by finite M and frequent spatial variation of the orientation of magnetic moments within the F layer.

Finally, Fig. 5(c) shows a distribution of magnetic moments and corresponding phase difference in the F layer relaxed from the originally curled state with orientation set by $\vec{m}(x,y) = [-(y-y_0),(x-x_0),0]/\sqrt{(x-x_0)^2+(y-y_0)^2}$, where (x_0,y_0) is the coordinate of the F barrier center. This state can be obtained by cooling the MJJ through the Curie temperature of the F layer under high current applied through the MJJ, since the uniformly distributed current flow in a square junction provides a similar vortex distribution of current-induced magnetic field. This magnetic state is a vortex with $\vec{M} = 0$, providing fluxometric $I_c = 1$. Vortex distribution of magnetization yields GLS $I_c \simeq 0.37$, i.e., by factor of almost 3 smaller. This factor is provided by a D-shape distribution of phase difference where the current actually flows in areas along the diagonals, while the countercurrent is distributed in neighboring D regions. Therefore, if a complex curling state appears in experiment at any stage during magnetization reversal, it will provide features on a Fraunhofer-like $I_c(H)$ dependence incomprehensible for fluxometric consideration. These features can be accounted for by reconstructing the phase difference distribution only.

V. SUMMARY

We have demonstrated a numerical approach for simulation of the magnetization reversal process in magnetic Josephson

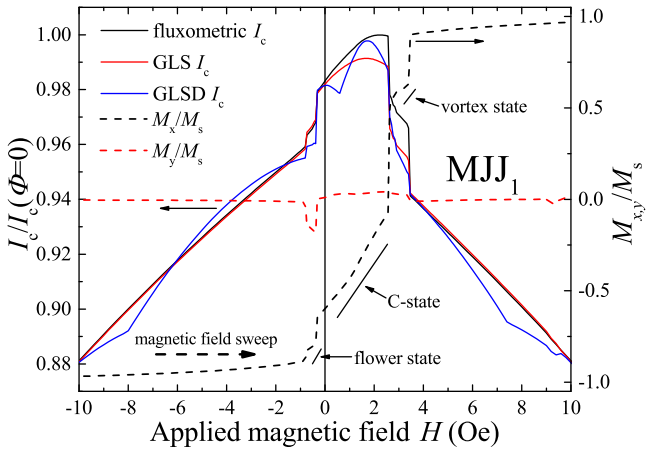

FIG. 6. Micromagnetic reconstructed dependencies of critical current on applied magnetic field for 1×1 μm^2 size MJJ$_1$ SFS. Dashed lines show field dependencies of corresponding projections of magnetization on principal axes.

junctions. Our model possesses only one extra free parameter which describes the magnetic stiffness of the F layer and justifies the experimentally observed coercive field. Based on micromagnetic simulation of magnetization reversal, we have provided three approaches for reconstruction of critical current dependence of lumped MJJs on applied magnetic field referred to as fluxometric reconstruction, GLS reconstruction, and GLSD reconstruction. The GLS and GLSD methods are based on reconstruction of actual phase difference distribution $\varphi(x,y,\vec{H})$ based on numerical methods of scalar reconstruction from a gradient field and employment of true dependence of the critical current on magnetic field [Eq. (5)]. All three approaches have shown a reasonable match with experiment.

We have considered rectangular MJJs with sufficient size aspect ratio and derived their critical current dependencies. It appears that rectangular MJJs can be employed as a memory element for Josephson magnetic memory where the logical state is set by the orientation of magnetic moment at zero applied magnetic field. Studying the $I_c(\vec{H})$ dependencies of rectangular MJJs at different angles of applied magnetic field, we have noted an impact of shape magnetic anisotropy of the F layer on the magnetization reversal process. A limit for the shape anisotropy effect is discussed.

Finally, we have derived critical currents of MJJ with the F layer relaxed to curling states at zero field. We showed that once a curling state in the F barrier occurs fluxometric reconstruction of I_c fails to derive the correct critical current.

Additionally, within this work, we have simulated a 1×1 μm^2 sized MJJ memory element. As an example, Fig. 6 shows $I_c(H)$ dependence for such MJJ$_1$ junction. We have employed the same $100\times100\times1$ mesh with the same internal magnetic stiffness as in Fig. 1(a) for calculations. Several well-pronounced features on $M_{x,y}(H)$ curves and corresponding steep transitions on $I_c(H)$ dependence are related to the magnetization reversal process through sequential flower, C, and vortex states. Magnetization reversal through well-defined curling macroscopic states is justified by a small size of the F layer. Hence, magnetic states and transitions can be effectively studied employing Josephson magnetometry with microscaled MJJs. Yet, the total variation of the critical current due to magnetization reversal does not exceed 0.05 and the variation in the $[-10$ Oe, $+10$ Oe$]$ range does not exceed 0.1 for both MJJ$_1$ and MJJ$_2$. Small I_c variation seems insufficient for rigid definition of memory logical states, making the minimization problem for MJJs based on $Pd_{0.99}Fe_{0.01}$ challenging.

Finally, we should discuss the legitimacy of the introduced internal magnetic stiffness. The IMS set with random anisotropies "mimics" a macroscopic characteristic of the ferromagnetic sample called the switching field distribution (SFD; see Refs. [36–38]). The SFD describes the width of the magnetization reversal process. In this work, we simply set the width to the dispersion of the normal distribution. As a result, first and second minima of reconstructed $I_c(H)$ in Fig. 1(a) mismatch slightly the experimental data. Once the SFD dispersion is determined it can be incorporated into the IMS ensuring a perfect match between reconstructed and experimental data.

ACKNOWLEDGMENTS

The authors acknowledge the Russian Foundation for Basic Research (RFBR) (Research Projects No. 16-32-00309, No. 16-32-60133, No. 15-52-10045, and No. 15-02-06743) and the Ministry of Education and Science of the Russian Federation in the framework of Increase Competitiveness Program of NUST "MISiS" (Research Projects No. K4-2014-080 and No. K2-2014-025). Experiments on MJJs for verification of the model have been supported by the Russian Science Foundation (RSF) Project No. 15-12-30030. V.S., M.Yu., and V.R. acknowledge partial support by the Program of Competitive Growth of Kazan Federal University. The authors acknowledge MIPT Data Center and Yuriy Shkandybin for providing computational capacity. The authors also acknowledge *in absentia* Matthew Harker and Paul O'Leary from University of Leoben, Austria, for employment of the numerical toolbox "Surface Reconstruction from Gradient Fields" available online.

[1] S. Oh, D. Youm, and M. Beasley, Appl. Phys. Lett. **71**, 2376 (1997).
[2] L. R. Tagirov, Phys. Rev. Lett. **83**, 2058 (1999).
[3] R. Held, J. Xu, A. Schmehl, C. W. Schneider, J. Mannhart, and M. Beasley, Appl. Phys. Lett. **89**, 163509 (2006).
[4] V. V. Bolginov, V. S. Stolyarov, D. S. Sobanin, A. L. Karpovich, and V. V. Ryazanov, JETP Lett. **95**, 366 (2012).
[5] V. V. Ryazanov, V. V. Bolginov, D. S. Sobanin, I. V. Vernik, S. K. Tolpygo, A. M. Kadin, and O. A. Mukhanov, Phys. Proc. **36**, 35 (2012).
[6] I. V. Vernik, V. V. Bol'ginov, S. V. Bakurskiy, A. A. Golubov, M. Yu. Kupriyanov, V. V. Ryazanov, and O. Mukhanov, IEEE Trans. Appl. Supercond. **23**, 1701208 (2013).

[7] S. V. Bakurskiy, N. V. Klenov, I. I. Soloviev, V. V. Bol'ginov, V. V. Ryazanov, I. V. Vernik, O. A. Mukhanov, M. Yu. Kupriyanov, and A. A. Golubov, Appl. Phys. Lett. **102**, 192603 (2013).
[8] V. V. Ryazanov, Phys. Usp. **42**, 825 (1999).
[9] V. V. Ryazanov, V. A.Oboznov, A. Yu. Rusanov, A. V. Veretennikov, A. A. Golubov, and J. Aarts, Phys. Rev. Lett. **86**, 2427 (2001).
[10] B. Baek, W. H. Rippard, S. P. Benz, S. E. Russek, and P. D. Dresselhaus, Nat. Commun. **5**, 3888 (2014).
[11] E. C. Gingrich, B. M. Niedzielski, J. A. Glick, Y. Wang, D. L. Miller, R. Loloee, W. P. Pratt Jr., and N. O. Birge, Nat. Phys. **12**, 564 (2016).
[12] A. A. Bannykh, J. Pfeiffer, V. S. Stolyarov, I. E. Batov, V. V. Ryazanov, and M. Weides, Phys. Rev. B **79**, 054501 (2009).
[13] K. K. Likharev and V. K. Semenov, IEEE Trans. Appl. Supercond. **1**, 3 (1991).
[14] D. S. Holmes, A. L. Ripple, and M. A. Manheimer, IEEE Trans. Appl. Supercond. **23**, 1701610 (2013).
[15] M. I. Khabipov, D. V. Balashov, F. Maibaum, A. B. Zorin, V. A. Oboznov, V. V. Bol'ginov, A. N. Rossolenko, and V. V. Ryazanov, Supercond. Sci. Technol. **23**, 045032 (2010).
[16] A. K. Feofanov, V. A. Oboznov, V. V. Bolginov, J. Lisenfeld, S. Poletto, V. V. Ryazanov, A. N. Rossolenko, M. Khabipov, D. Balashov, A. B. Zorin *et al.*, Nat. Phys. **6**, 593 (2010).
[17] M. Weides, M. Kemmler, E. Goldobin, D. Koelle, R. Kleiner, H. Kohlstedt, and A. Buzdin, Appl. Phys. Lett. **89**, 122511 (2006).
[18] A. V. Shcherbakova, K. G. Fedorov, K. V. Shulga, V. V. Ryazanov, V. V. Bol'ginov, V. A. Oboznov, S. V. Egorov, V. O. Shkolnikov, M. J. Wolf, and D. Beckmann, Supercond. Sci. Technol. **28**, 025009 (2015).
[19] I. I. Soloviev, N. V. Klenov, S. V. Bakursky, V. V. Bol'ginov, V. V. Ryazanov, M. Yu. Kupriyanov, and A. A. Golubov, Appl. Phys. Lett. **105**, 242601 (2014).
[20] I. I. Soloviev, N. V. Klenov, S. V. Bakursky, M. Yu. Kupriyanov, and A. A. Golubov, JETP Lett. **101**, 240 (2015).
[21] T. I. Larkin, V. V. Bolginov, V. S. Stolyarov, V. V. Ryazanov, I. V. Vernik, S. K. Tolpygo, and O. A. Mukhanov, Appl. Phys. Lett. **100**, 222601 (2012).
[22] S. V. Bakurskiy, N. V. Klenov, I. I. Soloviev, M. Yu. Kupriyanov, and A. A. Golubov, Phys. Rev. B **88**, 144519 (2013).
[23] J. E. Miltat and M. J. Donahue, *Handbook of Magnetism and Advanced Magnetic Materials* (John Wiley & Sons, Ltd., 2007), Vol. 2, p. 716, Chap. Numerical Micromagnetics: Finite Difference Methods.
[24] I. A. Golovchanskiy, V. V. Bol'ginov, N. N. Abramov, V. S. Stolyarov, A. B. Hamida, V. I. Chichkov, D. Roditchev, and V. V. Ryazanov, J. Appl. Phys. **120**, 163902 (2016).
[25] L. S. Uspenskaya, A. L. Rakhmanov, L. A. Dorosinskii, S. I. Bozhko, V. S. Stolyarov, and V. V. Bol'ginov, Mater. Res. Express **1**, 036104 (2014).
[26] Y. Nakatani, Y. Uesaka, and N. Hayashi, J. Appl. Phys. **28**, 2485 (1989).
[27] M. C. Chi and R. Alben, J. Appl. Phys. **48**, 2987 (1977).
[28] R. Alben, J. J. Becker, and M. C. Chi, J. Appl. Phys. **49**, 1653 (1978).
[29] J. Fidler and T. Schref, J. Phys. D: Appl. Phys. **33**, R135 (2000).
[30] L. Huang, M. Idir, C. Zuo, K. Kaznatcheev, L. Zhou, and A. Asundi, Opt. Lasers Eng. **64**, 1 (2015).
[31] M. Harker and P. O'Leary, Comput. Indus. **64**, 1221 (2013).
[32] Y. Li, Y. Lu, and W. E. Bailey, J. Appl. Phys. **113**, 17B506 (2013).
[33] A. Aharoni, L. Pust, and M. Kief, J. Appl. Phys. **87**, 6564 (2000).
[34] A. Aharoni, J. Appl. Phys. **83**, 3432 (1998).
[35] M. Vroubel, Y. Zhuang, B. Rejaei, J. N. Burghartz, A. M. Crawford, and S. X. Wang, IEEE Trans. Magn. **40**, 2835 (2004).
[36] I. A. Golovchanskiy, S. A. Fedoseev, and A. V. Pan, J. Phys. D: Appl. Phys. **46**, 215502 (2013).
[37] H. Zeng, S. Sun, T. S. Vedantam, J. P. Liu, Z.-R. Dai, and Z.-L. Wang, Appl. Phys. Lett. **80**, 2583 (2002).
[38] P. E. Kelly, K. O'Grady, P. I. Mayo, and R. W. Chantrell, IEEE Trans. Magn. **25**, 3881 (1989).